*Journal of Thermal Analysis and Calorimetry, Vol. 81 (2005) 425–433*

# THERMAL BEHAVIOR OF SHORT-RANGE-ORDER IN QUENCHED Cu–12 at% Mn ASSESSED BY DSC

*E. Donoso, G. Díaz and A. Varschavsky*[*]

Universidad de Chile, Facultad de Ciencias Físicas y Matemáticas, Instituto de Investigaciones y Ensayes de Materiales, Casilla 1420, Santiago, Chile

The ordering behavior of quenched Cu–12 at% Mn was investigated by differential scanning calorimetry (DSC) under increasing temperature conditions. The ordering process can be better explained in terms of a homogeneous short-range-order (SRO) rather than a disperse-short-range-order (DSRO) model as for concentrated Cu–γMn solid solutions. At the employed high quench rates ordering is established in one stage here termed stage 1, assisted by excess vacancies. This stage obeys a first order kinetics law, being the effective activation energy consistent with a weighed average sum of the activation energy for migration of free and bound vacancies. An estimated solute-vacancy binding energy of 15 kJ $mol^{-1}$ seems quite reasonable for this alloy together with the assessed activation energy for complex migration of 92.6 kJ $mol^{-1}$. By adopting a first SRO order parameter based in quasi-chemical theory in pair approximation and using boundary values calculated from displayed features of DSC traces, the retained degree of quenched-in order at room temperature was calculated. This procedure also enabled to estimate an ordering energy of –2.7 kJ $mol^{-1}$. The effect of quenching temperature demonstrate that for smaller vacancy sink densities, the retained degree of order at room temperature goes through a minimum.

***Keywords:*** *bound vacancies, Cu–12 at% Mn, DSC, kinetics, quenched, short-range-order, vacancies*

## Introduction

Much work has already been done on CuMn alloys, partly because of great technical interest in the mechanical, electrical and magnetic properties of this alloy system. In a recent paper [1] we reported calorimetric studies of disperse-short-range-order (DSRO) in a Cu–20 at% Mn alloy in which ordering phenomenon is a process leading to a stable and heterogeneous microstructure. This state has been also referred to occur in Cu–γMn concentrated solid solutions [2–4]. It was characterized by the presence of highly ordered particles embedded in a disordered matrix, exhibiting a $Cu_3Mn$ structure [2].

On the contrary, it has been reported that in dilute solid solutions [5–9] of other copper based alloys a short-range-order (SRO) situation prevails. It is characterized by an orderliness of structure which extends over short distances only, in any direction of the alloy system. In spite of the profuse research work still currently performed on CuMn alloys [10–17], only scarse information exists on SRO behavior in dilute and moderate dilute solid solutions [3–18]. We have chosen for this study a Cu–12 at% Mn alloy, which falls outside the possible existing γ'and γ'' phase boundaries [3], and close to the left limit of the enveloping ordered ε phase domain also reported [19], as shown in Figs 1a and b. In this way the alloy under study exhibit almost SRO only. On the other hand, this alloy composition is high enough to perform high accuracy measurements of ordering effects regardless of the experimental technique employed. At this alloy concentration (12 at% Mn) it has also been reported the interesting fact that the ordering energies of the second coordination sphere seem to be important as compared with the ordering energies of the first coordination sphere [20].

Specially differential scanning calorimetry (DSC) has been proved to be a useful tool in studying the temperature and time dependence of SRO [1, 5], because here a great accuracy for microstructural changes is combined with a relative great experimen-

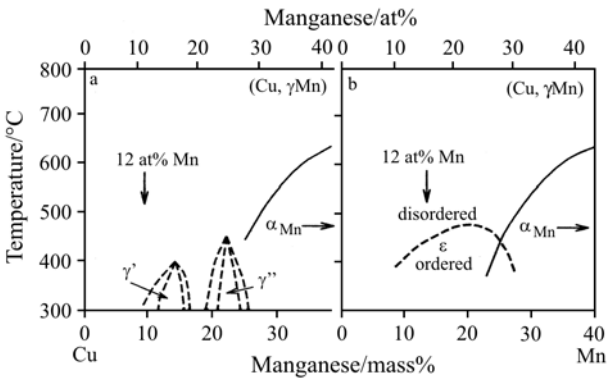


**Fig. 1** Two versions of the copper rich edge of the Cu–Mn system a – [3] and b – [19]

* Author for correspondence: avarscha@cec.uchile.cl

*1388–6150/$20.00*

*Akadémiai Kiadó, Budapest, Hungary*
*Springer, Dordrecht, The Netherlands*

tal simplicity. In this way it is possible to study extensively the temperature dependence of most of SRO features. In addition, although research work on ordering phenomenon in Cu–γMn continues [1], there are comparatively few studies on the non-isothermal kinetics of the SRO process from a quantitative treatment of DSC curves. Besides, no systematic research concerning quantitative evaluation of SRO during quenching and reordering until equilibrium is reached have been reported hitherto. There is also a need to examine the role of solute-vacancy complexes in the ordering process to the end of explaining the observed features displayed by the differential scanning calorimetric traces.

Chiefly the main scope of the present work is to analyze, on the basis of some theoretical approaches, thermodynamic and kinetic data from DSC traces of a Cu–12 at% Mn alloy. In particular the objectives of such an analysis are:

a) to determine whether during non-isothermal experiments performed in quenched alloys a homogeneous rather than a heterogeneous SRO state is developed

b) to determine the kinetic parameters of the ordering reactions and the effect of bound vacancies

c) to assess values for solute-vacancy binding energy, ordering energy for the first coordination sphere and activation energy for migration of bound vacancies

d) to compute boundary values for the first SRO parameter from the features displayed by the DSC traces for different quenching temperatures (thus enabling the capabilities of the technique to be enhanced)

## Experimental

The alloy studied contained 12 at% manganese. It was prepared in a Baltzer VSG 10 vacuum induction furnace from electrolytic copper (99.95 mass%) in a graphite crucible. The ingot was subsequently forged at 923 K to a thickness of 10 mm, pickled with a solution of nitric acid (15% in distilled water) to remove surface oxide, annealed in a vacuum furnace at 1123 K for 36 h to achieve complete homogeneity, and cooled in the furnace to room temperature. It was then cold-rolled to a thickness of 1.5 mm with intermediate annealing periods at 923 K for 1 h. After the last anneal, the material was finally rolled to a thickness of 0.75 mm (50% reduction).

Subsequent heat treatments were performed at different temperatures for 1 h, followed by quenching in a high rate quenching device developed in our laboratory. The quench time was measured with an oscilloscope and estimated in 200 ms. Such high quench rates were used in order to promote a one-stage ordering process via an excess of free and bound vacancies from all selected quenching temperatures. That is, by minimizing defect losses during the quench, sufficient defects in excess are available to reach an equilibrium state of SRO. Otherwise, reordering involves two-stage processes, the first assisted by excess defects and the second by equilibrium defects [1, 21, 22]. A one-stage ordering process facilitates to visualize the roles of unbound and bound vacancies.

Microcalorimetric analysis of the samples was performed in a DuPont 2000 thermal analyzer. Specimen discs 0.75 mm in thickness and 6 mm in diameter were prepared. Differential scanning calorimetric measurements of the heat flow were made by operating the calorimeter in the constant heating rate mode (heating rates of 0.667, 0.50, 0.33, 0.167 and 0.083 K $s^{-1}$). Runs were made from room temperature to 740 K. The details of the method employed for processing DSC traces is given in previous works [1, 5].

## Results and discussion

*Differential scanning calorimetric results*

Typical curves for the alloy under study are shown in the differential heat capacity $\Delta C_p$ *vs.* temperature $T$, curves at the indicated heating rates $\phi$ in Fig. 2. They are characterized by one exothermic peak namely stage 1 and one endothermic peak, stage 2. Stage 1 has been reported in the literature in connection with SRO development assisted by the migration of excess vacancies, while stage 2 was associated with a disordering process [22–25]. Further, the relative dominances of the different stages are independent of the heating rate. These features reflect that the reactions are dominated by kinetic rather than by thermodynamic factors. A kinetically dominated dissolution process is expected for a homogeneous SRO state or from the dissolution of particles taking place by a second-order transition [23]. However, in the latter case, the width and height of stage 2 would be dependent on the heating rate [26]. If the dissolution occurs by a first-order transition as in a DSRO state in αCu–Al alloys, where ordered domains are based on the $Cu_3Al$ structure [27, 28], such a process would be thermodynamically dominated, and hence the peak temperature of stage 2 would be independent of the heating rate. None of these features are observed in Fig. 2. This last type of behavior has been reported during non-isothermal scans for two-stage ordering in alloys exhibiting heterogeneous order [29, 30]. Therefore the observed heating rate dependence of the peak temperature of stage 2 and its associated shape invariability is in favour of disordering of a homogeneous SRO state.

The areas under the $\Delta C_p$ *vs*. $T$ curves which correspond to the enthalpies of the different reactions in

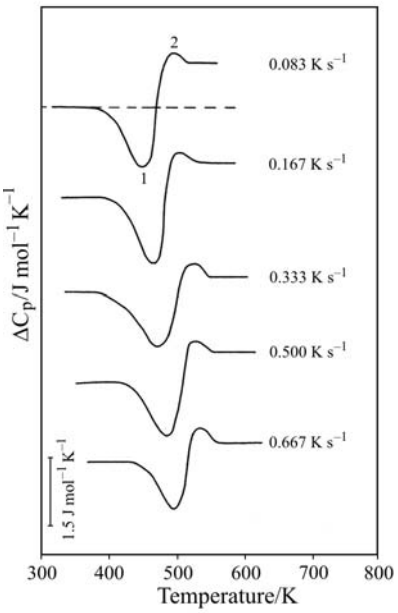


**Fig. 2** DSC curves for a Cu–12 at% Mn alloy quenched from 1073 K; stages 1 and 2 and ϕ are indicated

stage 1 and 2 are on average $\Delta H_1$=64±4 J mol$^{-1}$ and $\Delta H_2$=48±3 J mol$^{-1}$, being both essentially independent of the heating rate. The enthalpy absorption associated with stage 2 was evaluated by considering the area of the $\Delta C_p$ *vs*. *T* curve between the temperature at which the curve of stage 1 crosses the baseline, and the temperature at which energy is absorbed at a constant rate from the baseline. The enthalpy of exotherm 1 was determined by integrating the area below the maximum in the DSC scan.

In order to have a deeper insight of all these processes, a kinetic study will be next performed.

*Kinetic parameters and kinetic laws*

Before the integrated kinetic function which adjusts better to the experimental data obtained from a DSC trace is established, it is necessary to point out that, for a particular reaction if the reacted fraction is *y* at time *t*, in DSC, $dy/dt=(1/A)(da_t/dt)$, where $da_t/dt$ is the rate of heat flow, $a_t$, is the area under the peak at time *t*, and *A* is the total area. Values for effective activation energies are required as a necessary input in order to perform the non-isothermal kinetic analysis. These values were computed using the modified Kissinger's peak shift method [31],

$$\ln\left(\frac{T_p^2}{\phi}\right)=\frac{E}{RT_p}+\ln\left(\frac{E}{Rk_0}\right) \qquad (1)$$

Figure 3 shows the dependence of $\ln(T_p^2/\phi)$ *vs*. $1/T_p$ for the two stages where $T_p$ is the peak temperature,

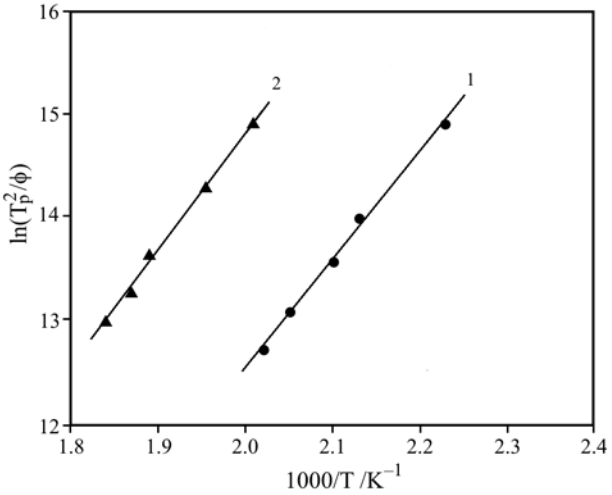


**Fig. 3** Modified Kissinger plots for stages 1 and 2

$k_0$ the pre-exponential factor, ϕ the heating rate and *R* the universal gas constant. The corresponding lines with slopes *E*/*R* allow one to evaluate the effective activation energy *E* for each process. These values which represent the average of 5 DSC runs are listed in Table 1.

It can be seen from Table 1 that activation energy for stage 1, although somewhat higher is consistent with that for vacancy migration [32], this fact will be discussed later on. It can also be seen that activation energy for disordering is practically the same than the one computed for stage 1. This finding is inconsistent with a diffusion-controlled nucleation and growth of ordered particles in a disordered matrix. If it were so, ordering rates slower that disordering rates would be expected; this is not the case in the present work.

The next step consists in adjusting a suitable law to the experimentally reacted fraction for stage 1. A mechanism-non-invoking method will be assumed [33]. The integrated kinetic approach under non-isothermal conditions gives:

$$\frac{1-(1-y)^{1-n}}{1-n}=k_0\theta(T) \qquad (2)$$

where *n* is the order of reaction [33] and θ(*T*) is the reduced time (the time at which the reaction goes to completion at an infinite temperature). Its value can be calculated from [31]:

$$\theta(T)=\frac{RT^2}{\phi E}\exp\left(-\frac{E}{RT}\right) \qquad (3)$$

**Table 1** Values of *E* and $k_0$ from modified Kissinger plots for stages 1 and 2 in Cu–12 at% Mn quenched from $T_q$=1073 K

| Stage | *E*/kJ mol$^{-1}$ | $k_0$/s$^{-1}$ |
|---|---|---|
| 1 | 89.5 | $4.6\cdot10^9$ |
| 2 | 91.3 | $6.5\cdot10^9$ |

In order to calculate the reduced time effective activation energy value was introduced in Eq. (3), thus allowing one to determine $\theta(T)$ along the temperature ranges where stage 1 peak is displayed.

Equation (1) applies for all values $n$, except $n$=1 (first order kinetics) for which the equation is

$$\ln\left(\frac{1}{1-y}\right) = k_0\theta(T) \tag{4}$$

Equation (2) was tested for the present data with unsuccessful results. However, it was possible to compute a process frequency factor from a plot of $\ln[1/(1-y)]$ *vs.* $\theta(T)$. This plot which is not shown here for brevity sake, resulted in a straight line of slope $k_0$, its value being $3.3\cdot10^9$ s$^{-1}$. Such plot was drawn for a specimen quenched from $T_q$=1073 K using a heating rate $\phi$=0.167 K s$^{-1}$. It was found that $k_0$ decreases somewhat as the heating rate employed increased, reaching an extrapolated maximum value of $3.9\cdot10^9$ s$^{-1}$ approximately when $\phi\rightarrow0$, which is independent of kinetically induced peak shifting effects. It is worth noting that this extrapolated value is closer to that calculated from Kissinger modified plot.

The pre-exponential factor was also calculated according to the relation:

$$k_0(\phi) = \frac{1}{\theta(T_p)} \tag{5}$$

For instance, for a specimen quenched from 1073 K using $\phi$=0.167 K s$^{-1}$, $T_p$=469 K and a value $k_0$=$1.1\cdot10^9$ s$^{-1}$ resulted, which is a good approximation to the values previously estimated. Further Eq. (5) allows to express the first order non-isothermal kinetics law in the normalized non usual form:

$$y = 1 - \exp\left(-\frac{\theta(T)}{\theta(T_p)}\right) \tag{6}$$

for a particular DSC trace. Marginally, it is worth noting that $\theta(T)/\theta(T_p)$ has its homologous in $t/\tau$ for the isothermal case, being $\tau$ the relaxation time. Such equation also fits quite well the experimental $y$ values calculated from DSC traces. Altogether, the method which employs Eq. (2) seem more reliable because $E$ was calculated separately. The calculated values of $k_0$ are in reasonable agreement under consideration of the different methods used in their determination.

Furthermore for a first order kinetic law $k_0=\eta c_t(T_q)\nu_{om}$ for non vacancy decay during the ordering process, where $\eta$ is an efficiency factor, $c_t(T_q)$ is the total vacancy concentration at the quenching temperature $T_q$ and $\nu_{om}$ is the pre-exponential factor for the equation governing the number of jumps per second a vacancy make. However for complete vacancy decay during the return of SRO, $k_0=(\eta c_t(T_q)\nu_{om})/2$ can be roughly estimated, if the classical mathematical structure of the first order kinetic law has to be preserved [21, 22]. Otherwise this structure modifies and a continuous variation of $k_0$ with temperature should be considered [5]. Vacancy concentration at quenching temperature $T_q$ is given by $c_t(T_q)=c^*\exp(-E_{ef}/RT_q)$; by taking $c^*$=2 and $E_{ef}$=96.3 kJ mol$^{-1}$ as the effective activation energy for vacancy formation calculated according to [5], $c_t(T_q)=4.1\cdot10^{-5}$ for $T_q$=1073 K. The pre-exponential factor is given by $\nu_{om}=Z\nu_0\exp(\Delta S_m/R)$, where $Z$=12 is the coordination number, the Debye frequency $\nu_0=10^{13}$ s$^{-1}$ and $\exp(\Delta S_m/R)$=2, being $\Delta S_m$ the activation entropy for vacancy migration. With the above data, $k_0=9.8\cdot10^9$ s$^{-1}$ is obtained. Such value strongly suggests that vacancy decay takes place during ordering as compared with all calculated values of $k_0$ in the present work, although is not possible to predict in what extent it does occurs.

*Binding energy of solute-vacancy complexes*

Solute-vacancy binding in Cu–γMn alloys may be important regarding the effective vacancy mobility. In general the binding effect arises from two factors: size factor and electronic factor [34]. The size factor is responsible for the strain field being produced by the size mismatch for oversized solute elements such that the lattice strain so produced is minimized by solute-vacancy atom association. The electronic factor, on the contrary, is considered to be prevalent in the presence of a solute element of valency higher than that of the host element. In the case of Cu–γMn alloys, at least the second factor is present since the Mn valence is higher than that of Cu, being the Mn size sligthly smaller. Hence a non-negligible binding energy may arise in a Mn-vacancy complex. The ratio of activation energy for vacancy formation and vacancy migration is about 1.3 as in all pure metals and alloys. $E_{sd}$, the activation energy for interdiffusion, which is estimated from the Brown and Ashby correlations [32], yields $E_f$=103.8 and $E_m$=79.8 kJ mol$^{-1}$ for 12 at% Mn. As all expressions relating the effective vacancy formation energy to solute-vacancy binding energy $B$ are valid only for dilute alloys, interpolated values for $E_f$ are required. For 8.0 and 5.0 at% Mn one obtains 104.1 and 104.8 kJ mol$^{-1}$, respectively, assuming that for pure copper the activation energy for vacancy formation is $E_v^f$=106.4 kJ mol$^{-1}$ [25]. The interpolated values for $E_f$ were substituted into [35]:

$$E_f = E_v^f - B\left[\frac{1-12\bar{c}}{12\bar{c}}\exp\left(-\frac{B}{RT_q}\right)+1\right]^{-1} \tag{7}$$

where $\bar{c}$ is the solute concentration and $T_q$ the quenching temperature. It can be seen that $E_f$ is not a linear

function of $T_q$. However, it is found experimentally through measurements of excess resistivity $\Delta\rho_a$ introduced by quenching that, for varying quench temperatures over a sufficiently narrow range of values of $T_q$, $d[\ln(\Delta\rho_a)]/d(1/T_q)=-E_f/R$. Iteratively calculated values of $B$ for 8.0 and 5.0 at% Mn alloys quenched from 1073 K give 16.4 and 13.6 kJ mol$^{-1}$. The average value of

$$B=15.0 \text{ kJ mol}^{-1}$$

was taken. Such a value is considered high enough in that an important fraction of atoms might be bound [36]. For instance, for Cu–12 at% Mn these less mobile complexes increase the effective activation energy $E$ for vacancy migration compared with calculated values for the activation energy of migration of monovacancies [32].

*Activation energy for migration of bound vacancies*

By considering the importance that bound vacancies may have during the ordering process, an estimate of the activation energy for bound vacancy migration $E_c$ will be made below. In fact, the effective rate constant [7, 37], at which order is established for a point defect mechanism, which is supposed to include bound unbound vacancies, is related to the total instantaneous defect concentration $c_t$, and to the effective mean rate at which defect atom exchange occurs, that is by $k_t(T)=c_t(T)\nu_t(T)$ in which $\nu_t(T)=\nu_{ot}\exp(-E/RT)$, $\nu_{ot}$ being the effective jump frequency constant. Here it will be considered that $c_t$ ($=c_u+c_b$) is equal to the sum of unbound and bound vacancy concentrations. Now, for simultaneous unbound and bound vacancy mechanisms an effective rate constant can be defined as [7, 38] $k_t=\nu_u c_u+\nu_b c_b$. Here $\nu_u$ and $\nu_b$ are the jump frequencies of unbound and bound vacancies, that is, $\nu_t(c_u+c_b)=\nu_u c_u+\nu_b c_b$. The idea contained in the last expression is that the entire population of vacancies, unbound and bound, is assigned one effective jump frequency $\nu_t$, which is obtained as a weighed sum of simpler jump frequencies describing individual processes. Hence:

$$\nu_t=\nu_u[1-\psi_b(T)]+\nu_b\psi_b(T) \quad (8)$$

in which $\psi_b(T)=c_b/c_t$ [39] here termed equilibrium transfer function, can be stated as:

$$\psi_b(T)=\frac{Z\bar{c}\exp(B/RT)}{1-(Z+1)\bar{c}+2Z\bar{c}\exp(B/RT)} \quad (9)$$

where $Z$ is the coordination number.

The simpler jump frequencies are given by $\nu_u=\nu_{om}\exp(-E_m/RT)$ and $\nu_b=\nu_{om}\exp(-E_c/RT)$, being $E_m$ the activation energy for migration of monovacancies, which amounts 79.8 kJ mol$^{-1}$ [32] and $E_c$ the activation energy for migration of bound vacancies. The attempt frequency $\nu_{om}$ is considered to be the same for unbound and bound vacancies and also equal to the composite attempt frequency $\nu_{ot}$ [37]. Therefore, the effective attempt frequency can be safely taken also as $\nu_{om}=12\nu_0\exp(\Delta S_m/R)$ for f.c.c. alloys, where $\nu_0$ is the Debye frequency and $\Delta S_m$ the activation entropy of migration of free vacancies [40]. Hence, from Eq. (8) it can be obtained the expresion:

$$\frac{E_c}{R}\frac{1}{T}=\ln\left\{\frac{\psi_b(T)}{\exp\left(-\frac{E}{RT}\right)-[1-\psi_b(T)]\exp\left(-\frac{E_m}{RT}\right)}\right\} \quad (10)$$

It was assumed that a quasi-equilibrium concentration exists between free and bound vacancies during development of stage 1 until true dynamic equilibrium is attained at the end temperature of the reaction. Designating by $\Lambda(T)$ the logarithmic term, a plot of $\Lambda(T)$ *vs*. $1/T$ resulted in a straight line as shown in Fig. 4. The slope of this line $E_c/R$, gives:

$$E_c=92.6 \text{ kJ mol}^{-1}$$

In this way, effective activation energy obtained by the modified Kissinger method [7, 31] from DSC traces can be written as a weighed sum of $E_m$ and $E_c$, that is, $E=\beta E_m+(1-\beta)E_c$ in which $\beta$ is the weighing factor. Its value amounts 0.24 for the alloy under study, thus meaning that the contribution of bound vacancies is important during the ordering process. If it is further considered that $E_c=E_m+\gamma B$, a value of $\gamma=0.85$ is obtained in the present case, thus indicating complex stability. It is worth noticing that when $\gamma=1$, $E_c$ becomes the activation energy for solute-vacancy complex dissolution [41], and when $\gamma=0$, no complexes exists at all.

*Retained degree of order and ordering energy from DSC traces*

The change of internal energy in copper based alloys, can be described entirely by the first SRO parameter

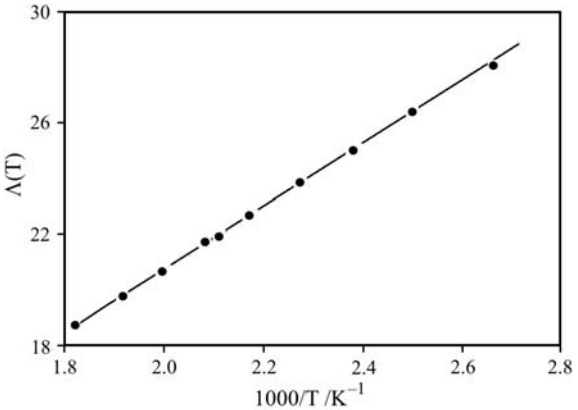


**Fig. 4** Function $\Lambda(T)$ *vs*. the reciprocal of temperature

[42]. Hence the transformed fraction for stage 1 can be expressed as $1-y=(\alpha-\alpha_E)/(\alpha_{T_2}-\alpha_E)$, where $\alpha$ is the instantaneous value of the short-range-order parameter, $\alpha_{T_2}$ is the equilibrium first SRO parameter when stage 1 goes to completion and $\alpha_E$ is the value retained after quenching. The temperature dependence of $\alpha$ is mostly independent of the SRO model chosen [4, 42]. We shall adopt an equilibrium Warren–Cowley parameter $\alpha = 1-(p^{e}_{Cu-Mn})/\bar{c}$ where $p^{e}_{Cu-Mn}$ is the conditional probability of finding a manganese atom next to a given copper atom and $\bar{c}$ is the concentration of manganese atoms. The superscript e denotes the equilibrium value. The conditional probability will be calculated from [43]:

$$p^{e}_{Cu-Mn} = \frac{-1+[1+4\bar{c}(1-\bar{c})(w^2-1)]^{1/2}}{2(1-\bar{c})(w^{-2}-1)} \quad (11)$$

where $w^2=\exp(2W/RT)$, being $W$ the ordering energy.

Boundary values for $\alpha_E$ can be estimated as follows. Since energy evolutions during the non-isothermal scans are due to the return of SRO and energy absorptions are due to the destruction of SRO, the degree of order present at room temperature after quenching may be specified in terms of an equivalent temperature $T_E$ at which these degrees of order would be in equilibrium [23]. In order to make the method straightforward, a schematic representation of a DSC trace is shown in Fig. 5. From this figure, for a given quenching temperature, $T_E$ can be calculated from a knowledge of the net absorption or evolution of energy up to some temperature at which a constant rate of destruction of order has been attained, and the rate of absorption of energy on continuous heating above such temperature. If $\Delta H_1(T_1,T_2)$, $\Delta H_2(T_2,T_e)$, are the energies associated with the respective peaks, and $\Delta H_e=\Delta C_{pe}(T_E-T_e)$ where $\Delta C_{pe}$ and $T_e$ represents the constant differential specific heat and the equilibrium temperature, at which energy commences to be absorbed at a constant rate, one has $\Delta H_E=\Delta H_1(T_1,T_2)-\Delta H_2(T_2,T_e)$, and hence

$$T_E = T_e + \frac{[\Delta H_1(T_1,T_2)-\Delta H_2(T_2,T_e)]}{\Delta C_{pe}} \quad (12)$$

On the other hand, the enthalpy change associated with a variation $\Delta\alpha=\alpha_E-\alpha_{T_2}$ of the SRO parameter taking place during the SRO return is given by [44, 45]:

$$\Delta H_1 = -\bar{c}(1-\bar{c})ZW\Delta\alpha \quad (13)$$

Using computational iterative methods, from the expression for $\alpha$, Eqs (11)–(13) ordering energy $W$, $T_E$ and hence the retained degree of order at room temperature specified by $\alpha_E$ can be determined. The average measured enthalpy value $\Delta H_1$ calculated from DSC traces of Fig. 2 amounts 64±4 kJ mol$^{-1}$. Ordering energy was calculated for a heating rate $\phi$=0.167 K s$^{-1}$ using the corresponding data listed in Table 2 of the next section for a quenching temperature $T_q$=1073 K, resulting in:

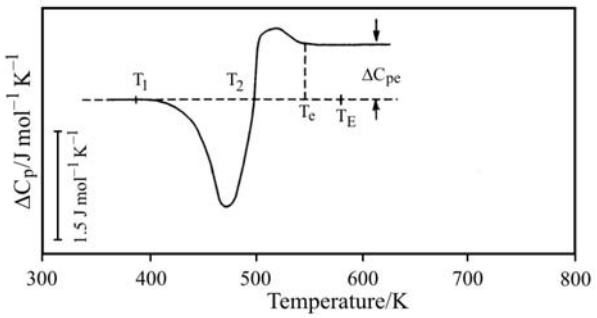


**Fig. 5** DSC curve showing a schematic representation of a one-stage SRO ordering process followed by a disordering stage in a quenched alloy. $T_E$, may be simply specified as the temperature 1 which the equilibrium degree of order corresponding to that temperature is retained at room temperature

$$W = -2.7 \text{ kJ mol}^{-1}$$

which is quite similar to other reported data [3, 46]. As it was confirmed, $W$ values are insensible to quenching temperature. It is interesting to point out also that $B+B'=2W$ [47], $B'$ being the Cu-vacancy binding energy which amounts to –20.4 kJ mol$^{-1}$, indicating strong repulsion.

*Effect of quenching temperature on boundary values of* $\alpha$

Figure 6 shows the DSC traces corresponding to specimens quenched from the indicated selected temperatures, $T_q$. In these DSC curves, the temperatures $T_1$, $T_2$ and $T_e$ were measured and $\alpha_E$ calculated together with $\Delta H_1$ as average values of 5 DSC runs. All relevant data are presented in Table 2. With above data, $-\alpha_{T_2}$, $-\alpha_E$ and $-\alpha_{T_q}$ were calculated. The resulsing values are plotted in Fig. 7.

In the above plot several points of interest arise:

- The degree of order present at room temperature after quenching at first decreases with quenching temperature and then increases again. Thus the maximum disorder is obtained around 1073 K. For quenches above this temperature less disorder is retained, so that on quenching from 1123 K the alloy is somewhat more ordered than on quenching from 973 K.

**Table 2** Values for $T_q$, $T_1$, $T_2$, $T_e$, $T_E$ and $\Delta H_1$ ($\phi$=0.167 K s$^{-1}$); data represent the average of 5 DSC runs

| $T_q$/K | $T_1$/K | $T_2$/K | $T_e$/K | $T_E$/K | $\Delta H_1$/J mol$^{-1}$ |
|---|---|---|---|---|---|
| 973 | 402 | 478 | 525 | 542 | 56±3 |
| 1073 | 392 | 491 | 534 | 556 | 64±4 |
| 1123 | 380 | 485 | 530 | 550 | 60±3 |

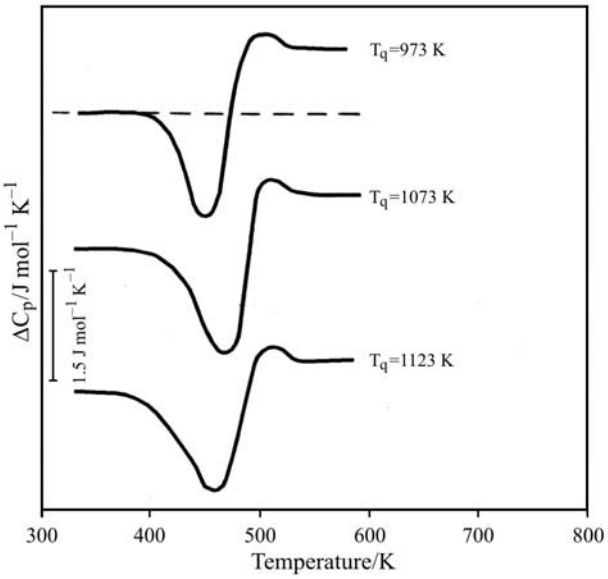


**Fig. 6** DSC traces for Cu–12 at% Mn quenched from the indicated temperatures; $\phi$=0.167 K s$^{-1}$

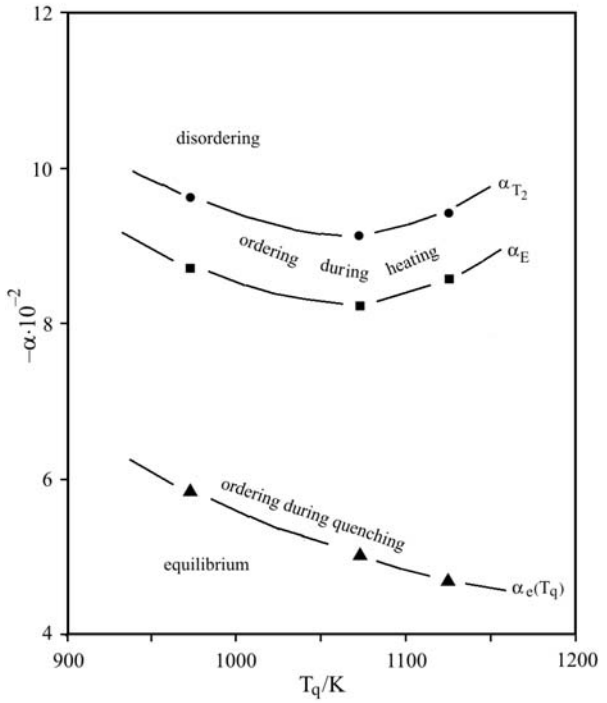


**Fig. 7** Values of the first SRO parameters $\alpha_e(T_q)$ (at quenching temperature), $\alpha_E$ (retained at room temperature) and $\alpha_{T_2}$ (at equilibrium temperature). The $\alpha$ value ranges where the indicated processes take place are also shown

- As the quenching temperature increase the degree of ordering which occurs during the quench becomes more marked. For instance, for the specimen quenched from 1123 K ($\alpha_{T_q}$ =–0.0484), ordering during the quench changes the degree of order from that in equilibrium at 1123 K to that in equilibrium at 550 K ($\alpha_E$=–0.089). The increase in the degrees of order, which can be specified by the values of $|\alpha_E - \alpha_{T_q}|$ are 0.029/0.0333/0.0367 for quenching temperatures of 973/1073/1123 K.

These features are of course limited by the loss of vacancies during the quench which at first approximation will be neglected in view of the high quench rates here employed. As the SRO process is controlled by the effective jumps to produce ordering, for a quenching temperature of 973 K less vacancies migrate, contrary to what occurs for 1123 K, where the amount of reordering is increased. For 1073 K the situation is intermediate. On the other hand, the higher is the quenching temperature the alloy is in a more disordered state at that temperature. A combination of these factors can explain the maximum degree of disorder found at room temperature for a quench from 1073 K. These results are similar to those obtained by resistivity measuremens in Cu–30Zn [25].

The temperature $T_2$ at which the transition occurs from an evolution to an absorption of energy at the end of stage 1 results from the attainment of the equilibrium degree of order at that temperature. The temperature at which disordered commences is of course a function of the degree of disorder retained at room temperature after quenching and of the concentration of quenched-in vacancies. A consideration of these two factors explain the increase and then the decrease in the temperature at which disordering starts after quenching from the different temperatures. Thus, when quenching from 973 K the degree of disorder retained is lower as is the vacancy concentration.

Reordering occurs until the equilibrium degree of order is reached at 478 K. On quenching from 1073 K more disorder is quenched-in, the vacancy concentration is still higher, so that the increased ordering during this stage enables the equilibrium degree of order to be attained at 491 K. For the quench from 1123 K less disorder is quenched-in than for quenches from 973 and 1073 K, but the vacancy concentration is higher than for either of these temperatures, so that considerable ordering occurs and the equilibrium degree of order is reached at 485 K. These results are consistent with the increase in order during the heating process measured by $|\alpha_{T_2} - \alpha_E|$ until equilibrium is reached and also a measure of the order developed. In fact $|\alpha_{T_2} - \alpha_E|$=0.0086/0.0095/0.0090 and $\Delta H_1$=56/65/60 kJ mol$^{-1}$ for quenching temperatures of 973/1073/1123 K.

It is also worthwhile to recall that depending upon the quenching conditions in other alloy systems such us $\alpha$Cu–Al, the ordering process can take place in two stages [21, 22]. The first one is associated with the migration of non-equilibrium vacancies and the second one with the migration of thermal vacancies.

The above analysis hold for relative low effective vacancy sink densities $\rho_t$ ($=\rho_d+\rho_g$) where $\rho_d$ is the sink density for dislocations and $\rho_g$ for gain boundaries. For the present well annealed alloy $\rho_t=6.7\cdot10^{-9}$ is assuming a dislocation density of $10^7$ cm$^{-2}$ and measuring a grain size of 100 μ. The sensitivity of the theoretical predictions to changes in sink density are investigated from a model previously developed by two of the authors [40] applied to this study. Such research work indicates that for higher sink densities, the retained degree of order decreases with increasing quenching temperatures, and the observed minimum disappears. A detailed discussion of this behavior is given in [40].

Finally, it is worth recalling that even if SRO effects are not larger in this alloy, the heat evolved during DSC runs should correspond to the return of SRO. If one supposes as a first approximation that the heat measured in the curve for an alloy quenched from 973 K, which is about 56 J mol$^{-1}$ (Fig. 6), would correspond to the annealing of quenched-in vacancies ($E_f$–$B$/2)=96.3 kJ mol$^{-1}$ (calculated by using the procedure given in [5] as said before), a quenched-in vacancy concentration extremely high of about $5.8\cdot10^{-4}$ is calculated, which results unrealistic for all quenching temperatures. So, the exothermic peaks observed would be associated unequivocally with the SRO return. The main reason for employing a semi-diluted alloy within the scope of the present work, is that the equilibrium equation for $\psi_b(T)$ (Eq. (9)) has restrictions in its use in concentrated alloys, thus turning less rigorous all above analysis. Further, for a more concentrated material, the ε ordered phase influence becomes to increase affecting the SRO state. On the other hand, as the dilution degree increases, SRO ordering features becomes drastically less marked in the DSC traces in this alloy system [2].

## Conclusions

The investigation of the ordering process in Cu–12 at% Mn by differential scanning calorimetry allowed to obtain kinetic data for a previously quenched alloy. The calculated effective activation energy was rationalized as a weighed average sum of the migration activation energies for free and bound vacancies. The number of these solute-vacancy complexes was important concerning this kinetic parameter. The process frequency factor value is in agreement with that expected from the development SRO during stage 1. A solute-vacancy binding energy of 15 kJ mol$^{-1}$ and a corresponding value of 92.6 kJ mol$^{-1}$ for the activation energy for migration were assessed. This last value was obtained by using a simple model for equilibrium distribution of vacancy concentrations.

The retained degree of order after quenching was estimated by adopting an equilibrium Warren–Cowley parameter, which was used in conjunction with a method developed for processing features displayed in DSC traces. Besides, a combination of such procedures, together with the use of enthalpimetric data allowed to estimate and ordering energy of –2.7 kJ mol$^{-1}$. Finally, the effect of quenching temperature and vacancy sink density was examined at the light of a previous work. All ordering features evaluated during non-isothermal heating thus enables to extend the capabilities of differential scanning calorimetry as a quantitative research tool.

## Acknowledgements

The authors would like to acknowledge the Fondo Nacional de Desarrollo Científico y Tecnológico (FONDECYT) for financial support, Project 1040795 and the Facultad de Ciencias Físicas y Matemáticas de la Universidad de Chile for the facilities provided for this research.

## References

1 A. Varschavsky and E. Donoso, J. Therm. Anal. Cal., 76 (2004) 853.
2 H. Warlimont, K. Bernecker and R. Luck, Z. Metallkd., 62 (1971) 816.
3 R. Reishsner and W. Pfeiler, J. Phys. Chem. Solids, 46 (1985) 1431.
4 W. Pfeiler, Acta Metall., 36 (1988) 2417.
5 A. Varschavsky, G. Díaz and E. Donoso, Mater. Sci. Eng., A 369 (2004) 1.
6 E. Donoso and A. Varschavsky, Mater. Sci. Eng., A 369 (2004) 10.
7 A. Varschavsky and E. Donoso, J. Therm. Anal. Cal., 73 (2003) 167.
8 A. Varschavsky and E. Donoso, J. Therm. Anal. Cal., 65 (2001) 185.
9 A. Varschavsky and E. Donoso, J. Therm. Anal. Cal., 63 (2001) 397.
10 A. Varschavsky and E. Donoso, Mater. Lett., 31 (1997) 329.
11 O. Engler, Acta Mater., 49 (2001) 1237.
12 O. Engler, Acta Mater., 48 (2001) 4827.
13 Q. Y. Pan, X. Lin, W. D. Huang, H. S. Zhou and G. L. Shang, Mater. Res. Bull., 33 (1998) 1621.
14 Q. Y. Pan, D. Huang, X. Lin and Y. H. Zhou, J. Cryst. Growth, 181 (1997) 109.
15 H. Roelofs, B. Schonfeld, G. Kostorz, W. Buhrer, J. L. Robertson, P. Zschack and G. E. Ice, Acta Metall., 34 (1996) 139.
16 H. Roelofs, B. Schonfeld, G. Kostorz and W. Buhrer, Phys. Stat. Solid., B, 187 (1995) 31.
17 A. Nortmann and Ch. Schwink, Scripta Metall. Materialia, 33 (1995) 369.
18 A. Varschavsky and E. Donoso, Mater. Lett., 31 (1997) 239.
19 Phase Diagrams of Binary Copper Alloys, ASM International. Monograph Series on Alloy Phase

Diagrams Eds P. R. Subromanian, D. J. Chakrabarty and D. E. Laughlin, Ohio 1994, p. 253.
20 T. M. Harders, T. J. Hicks and J. H. Smith, J. Phys. F, 13 (1983) 1262.
21 A. Varschavsky and E. Donoso, Mater. Sci. Eng., A 212 (1991) 95.
22 A. Varschavsky and E. Donoso, Thermochim. Acta, 203 (1992) 391.
23 S. Matsuo and L. M. Clarebrough, Acta Metall., 11 (1963) 1195.
24 C. Kinoshita, Y. Tomokiyo, H. Matsuda and T. Eguchi, Trans. Jpn. Inst. Met., 14 (1973) 91.
25 E. Donoso and A. Varschavsky, J. Thermal Anal., 45 (1995) 1419.
26 M. Van Rooyen, J. A. Sinte Maartensduk and E. Mittemeijer, Metall. Trans., A 19 (1988) 2433.
27 W. Gaudig and H. Warlimont, Z. Metallkd., 60 (1969) 488.
28 A. Varschavsky, M. I. Pérez and T. Löbel, Metall. Trans., A 6 (1975) 577.
29 K. Mitsui, Y. Mishima and T. Suzuki, Philos. Mag. A, 59 (1989) 123.
30 K. Mitsui, Philos. Mag. A, 53 (1986) 447.
31 E. J. Mittemeijer, Liu Ching, P. J. Van der Shaaf, C. M. Brakmann and B. M. Korevaar, Metall. Trans., 19 A (1988) 925.
32 A. M. Brown and M. F. Ashby, Acta Metall., 28 (1980) 1085.
33 K. N. Ninan, J. Thermal Anal., 35 (1989) 1267.
34 A. K. Mukhopdhyoy, G. J. Shiflet and E. A. Starke, Scr. Metall. Mater., 24 (1990) 307.
35 J. J. Takamura, M. Doyama and H. Kisinati, Point Defects and Defect Interactions in Metals, North-Holland, Amsterdam 1982, p. 452.
36 S. Ozbilen and H. M. Flower, Acta Metall., 37 (1989) 2993.
37 A. Varschavsky and E. Donoso, J. Min. Metall., 35 (1999) 255.
38 L. K. Mansur, Acta Metall., 29 (1981) 375.
39 D. V. Ragone, Thermodynamics of Materials, Vol. II, Wiley, New York 1995, p. 73.
40 A. Varschavsky and E. Donoso, Mater. Sci. Eng., A 212 (1996) 265.
41 A. D. LeClaire, J. Nucl. Mater., 69 (1978) 70.
42 C. H. Caceres and A. Blake, Phys. Status Solidi, A 194 (2002) 147.
43 S. Radelaar, J. Chem. Phys. Status Solids, 31 (1970) 16.
44 W. Pfeiler, P. Meisterle and M. Zehetbauer, Acta Metall., 32 (1984) 1053.
45 A. Vander Beukel and S. Radelaar, Acta Metall., 31 (1983) 419.
46 W. Pfeiler and R. Reihsner, Phys. Status, Solidi, A 97 (1986) 377.
47 F. W. Shapink, Philos. Mag., 12 (1965) 1055.

Received: October 1, 2004
In revised form: February 1, 2005

DOI: 10.1007/s10973-005-6557-3